Materials Characterization 139 (2018) 208–220

Contents lists available at ScienceDirect

Materials Characterization

journal homepage: www.elsevier.com/locate/matchar

Impact of targeted chemistries on maraging steel precipitation evolution observed using SANS and APT

V. Gray[a,*], D. Galvin[a], P. Hill[b], M. Rawson[b], K. Perkins[c]

[a] Institute of Structural Materials, Swansea University, Fabian Way, Skewen, Swansea SA1 8EN, UK
[b] Rolls-Royce plc., PO Box 31, Derby DE24 8BJ, UK
[c] College of Engineering, Swansea University, Fabian Way, Skewen, Swansea SA1 8EN, UK

ABSTRACT

Building on a previous study of the novel aerospace maraging steel known as F1E, SANS and atom probe tomography (APT) have been used to study three variant chemistries designed to impact the growth and development of either laves or β-phase precipitates. One chemistry reduced the available laves forming elements, Mo and W, resulting in a reduction in both austenitization and aging laves populations. A second chemistry reduced the β-phase forming element, Al, causing a reduction in the nucleating laves but not β-phase precipitates. Mechanical properties such as tensile, creep and hardness are examined with respect to the precipitate populations.

1. Introduction

Thermal aging treatments impact the growth and development of intermetallic precipitates within the martensitic matrix of low carbon-high strength iron based superalloys, these materials are more commonly classified as maraging steels where 'maraging' is coined from the combination of 'martensitic' and 'aging' [1]. The enhanced properties of these materials make them well suited to applications such as aerospace gears and shafts which are continually required to operate at higher stresses and temperatures with each new generation of engine [2]. Previously, small angle neutron scattering (SANS) was used to study the development and formation of precipitates in the novel maraging steel F1E [3] which has been found to out-perform current competing materials AerMet 100 and Super CMV [4].

Since the development of F1E by Rolls Royce plc in 2009, further work has been carried out to enhance this novel steel through varying the chemistry to target specific precipitates thought to contribute to desirable material properties. Our prior work on F1E [3,4], showed this steel to have three populations of precipitates; (i) a molybdenum-tungsten rich laves phase [$(Fe,Cr)_2$ (Mo,W)] present from austenitization, (ii) another laves population that nucleates and grows during aging, and, (iii) a nickel-aluminium rich β-phase (NiAl) which also nucleates and grows during aging. Each precipitate is expected to contribute to the observed mechanical properties with improvements in creep resistance and microstructural stability reportedly due to laves pinning the martensite lath boundaries, and further material strength arising from the β-phase precipitates [5,6].

Given the link of precipitates to mechanical properties, this work examines three variations to the original F1E chemistry [3] by quantifying the specific precipitate populations and their evolution during the aging process. To examine the impact of chemistry on laves precipitates two chemistries were examined with reduced Mo and W, one aiming for a ~25% reduction in laves, and, another aiming for a ~50% reduction or near elimination of laves precipitates. A third chemistry targeting the formation of β-phase was examined that had reduced Al. SANS was used to quantify the precipitate populations for a range of heat treatments using input from Atom Probe Tomography (APT) and Electron Microscopy techniques (SEM, TEM, STEM). By conducting tensile, creep and hardness test, these combination of structural data enable insight into the effect that specific precipitate populations have on mechanical properties.

2. Targeting Precipitation Through Chemistry

The three F1E variant chemistries examined in this work are referred to as F1E-LL, F1E-NL and F1E-Lβ with targeted LL = Low Laves, NL = No Laves and Lβ = Low βeta phases. Compositions of F1E and each variant chemistry are shown in Table 1.

The F1E and variants described in Table 1 were provided by Rolls-Royce plc. [7] in as forged bars manufactured by ATI Allvac, USA [8] using a VIM/VAR process before homogenisation and hot rolling to

* Corresponding author.
E-mail address: veronica.gray@qut.edu.au (V. Gray).

https://doi.org/10.1016/j.matchar.2018.02.045
Received 11 December 2017; Received in revised form 21 February 2018; Accepted 28 February 2018
Available online 05 March 2018

Table 1
General composition of maraging steel F1E in %wt. Chemistry variations highlighted in red.

	C	Cr	Mo	Ni	Al	Co	W	B	Fe
F1E	0.003	10	2.75	7	1.8	8.3	2.45	0.002	% Balance
F1E-Lβ	0.003	10	2.75	7	**1.2**	8.3	2.45	0.002	% Balance
F1E-LL	0	9	**2**	9	1.75	8.3	**2**	0.002	% Balance
F1E-NL	0	10	**1.4**	7	1.75	8.3	**1.2**	0.002	% Balance

Table 2
Composition of laves and β precipitates by %wt.

	C	Cr	Mo	Ni	Al	Co	W	Fe
Laves								
F1E	0.03	13.7	24.0	4.5	0.06	5.1	18.8	% Balance
F1E-Lβ	0.02	15.3	25.5	**3.6**	0.01	4.7	19.6	% Balance
F1E-LL	0.04	14.8	22.6	5.0	0.05	4.7	20.3	% Balance
F1E-NL	0.01	**35.6**	**11.9**	5.1	0.14	3.9	**4.7**	% Balance
β-Phase								
F1E	0.01	5.6	1.3	33.7	11.3	6.4	1.4	% Balance
F1E-Lβ	0.00	6.1	1.1	32.6	9.4	6.3	1.5	% Balance
F1E-LL	0.00	5.9	1.2	30.8	8.3	6.3	1.5	% Balance
F1E-NL	0.01	5.5	**0.7**	33.9	10.9	6.3	1.0	% Balance

Table 3
Difference in scattering length densities obtained from atom probe tomography at > 80% phase pure ($10^{-6}/Å^2$).

	Matrix	Laves	β-Phase
F1E-Lβ	6.99	6.16	5.52
F1E-LL	7.06	6.07	5.64
F1E-NL	7.03	6.10	5.39

eliminate any pre-existing precipitates. Cubes measuring 20 × 20 × 20 mm were then austenitized at the prescribed conditions for 1 h in a laboratory carbolite furnace before air-quenching to room temperature. They were then individually aged and processed for each observation technique as described in subsequent sections.

3. Precipitate Composition Via Atom Probe Tomography

APT was used to determine the chemical composition of the individual precipitates and to enable scattering length densities to be constrained in subsequent SANS analysis. Samples were prepared using electropolishing and focused ion beam (FIB) liftout. Matchsticks of 0.5 mm × 0.5 mm × 20 mm were electropolished using a solution of 25% perchloric acid and 75% glacial acetic acid at a DC voltage of 14 V until a neck formed allowing for separation into two needle-shaped specimens [9]. Needles were refined using a polishing solution of 2% perchloric acid in butoxyethanol. Precipitate compositions shown in Table 2 were taken at isosurfaces of > 8% Mo for laves, and, > 15%Ni for β-phase for samples aged for 5 h at 540 °C.

The impact of element availability on the chemistry of the precipitates is apparent from the APT composition data shown in Table 2:

- F1E-Lβ: the reduction in Al results in the laves having slightly higher Cr and reduced Ni content in comparison to F1E.
- F1E-LL: shows no significant variation from F1E.
- F1E-NL: the reduction in Mo and W is reflected in laves chemistry, with a significant increase in Cr for this variant.

It is supposed that due to the lack of Mo and the high diffusivity of Cr, the Cr substitutes in the laves precipitate linking to the earlier observation of the build-up of Cr during aging of F1E and previous studies from SANS and SEM [3].

For all chemistries there is little variation in β-phase composition with only a reduction in Mo seen for the F1E-NL when compared to F1E.

4. Heat Treatments

In this study a range of austenitization and aging heat treatments were used to evaluate the initial and long term impact chemistry variation had on precipitate development. For F1E the austenitization temperature of 960 °C was chosen as it was determined to be sufficient to dissolve all pre-existing laves and consequently avoid potential 'precipitate splitting' in F1E [3]. As such, for the modified chemistries austenitization temperatures were calculated using MTDATA [10] to be equivalent to 960 °C for F1E. All austenitization and aging conditions for F1E-Lβ, F1E-LL and F1E-NL are shown on the following graphs and listed in the Appendix.

5. SANS

Samples from SANS underwent preparation as described in Section 2 and heat treated as described in the SANS Results and Appendix. After heat treating, samples were then cut into squares of 10 × 10 mm and reduced to a thickness of 300 μm for optimal neutron transmission and minimise multiple scattering [3]. SANS was conducted on the QUOKKA at ANSTO, Australia [11]. Three configurations were used to cover a q range of ~0.003 to 0.74 $Å^{-1}$ where q is the magnitude of the scattering vector defined as $q = 4\pi/\lambda.sin\theta$, where λ = 5 Å with $\Delta\lambda/\lambda$ = 10% resolution and 2θ the scattering angle. The configurations were

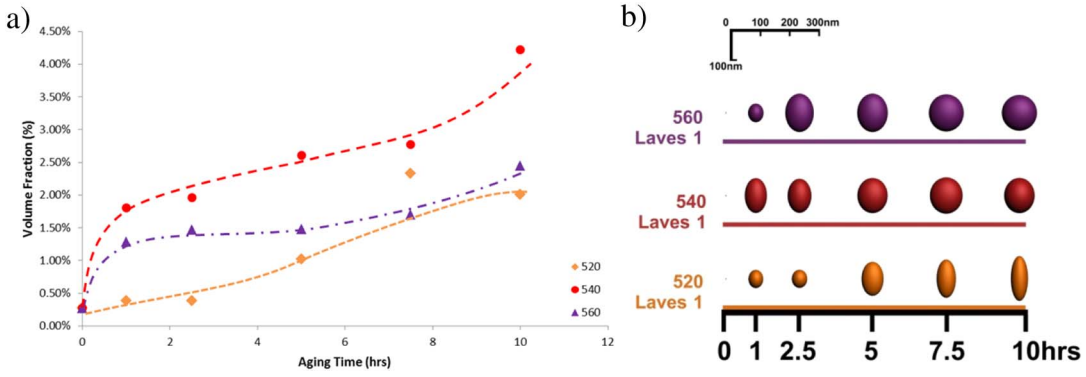

Fig. 1. F1E-Lβ Laves 1: aging temperature and time dependence a) volume fraction, and, b) size.

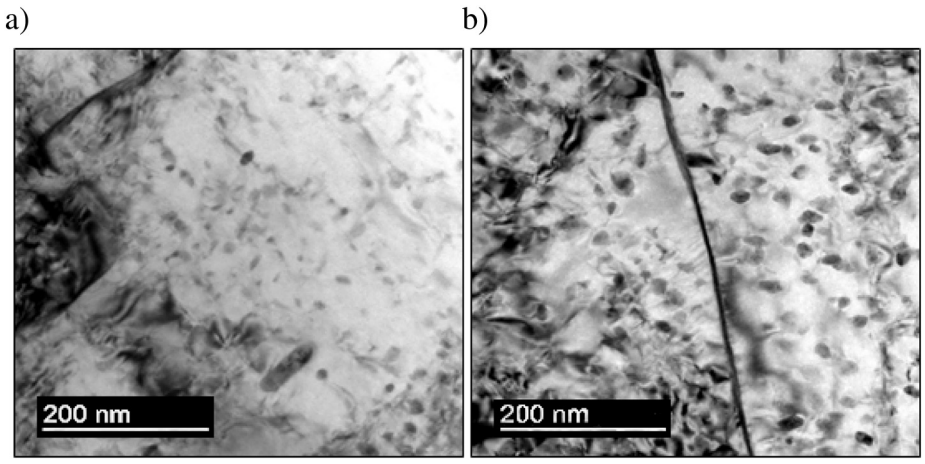

Fig. 2. F1E-Lβ Laves 1 via TEM aged for a) 1 h, and, b) 5 h.

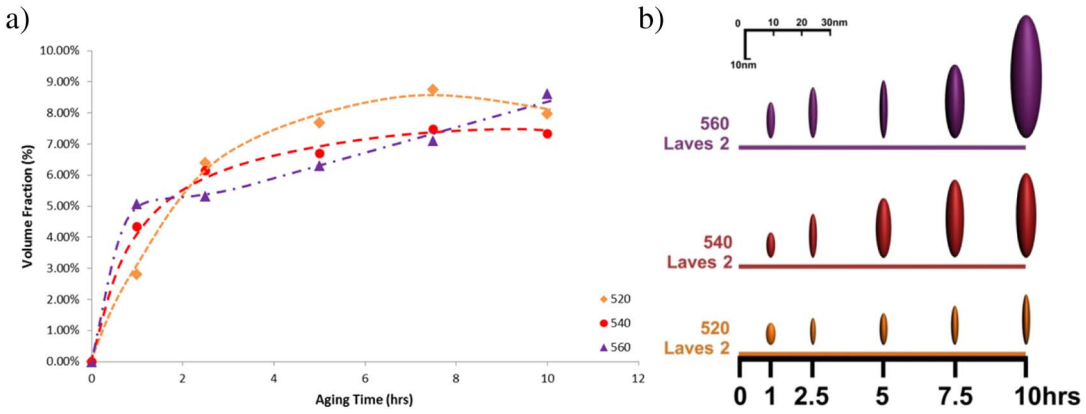

Fig. 3. F1E-Lβ Laves 2: aging temperature and time dependence a) volume fraction, and, b) size.

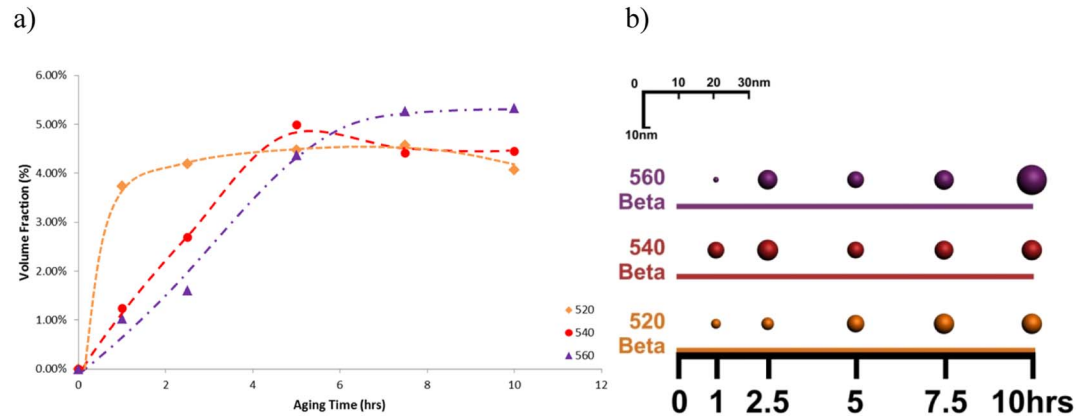

Fig. 4. F1E-Lβ β-phase: aging temperature and time dependence a) volume fraction, and, b) size.

$L_1 = L_2 = 20$ m, $L_1 = L_2 = 12$ m, and $L_1 = 12$ m $L_2 = 1.3$ m, where L_1 and L_2 are source-to-sample and sample-to-detector distances, and with source and sample apertures of 50 mm and 5 mm diameter respectively. The latter yielded an illuminated average sample volume of 6 mm^3.

SANS data were reduced using NCNR SANS reduction macros modified for the QUOKKA instrument, using Igor software package [12] and transformed to absolute scale by the use of an attenuated direct beam transmission measurement [13,14]. The spectra were then analysed using in-built algorithms within the SASview package [15–21].

In this experiment the total scattering exhibits both nuclear and magnetic scattering. The precipitates are non-magnetic while the matrix is ferromagnetic. In the variant chemistries examined, similar to

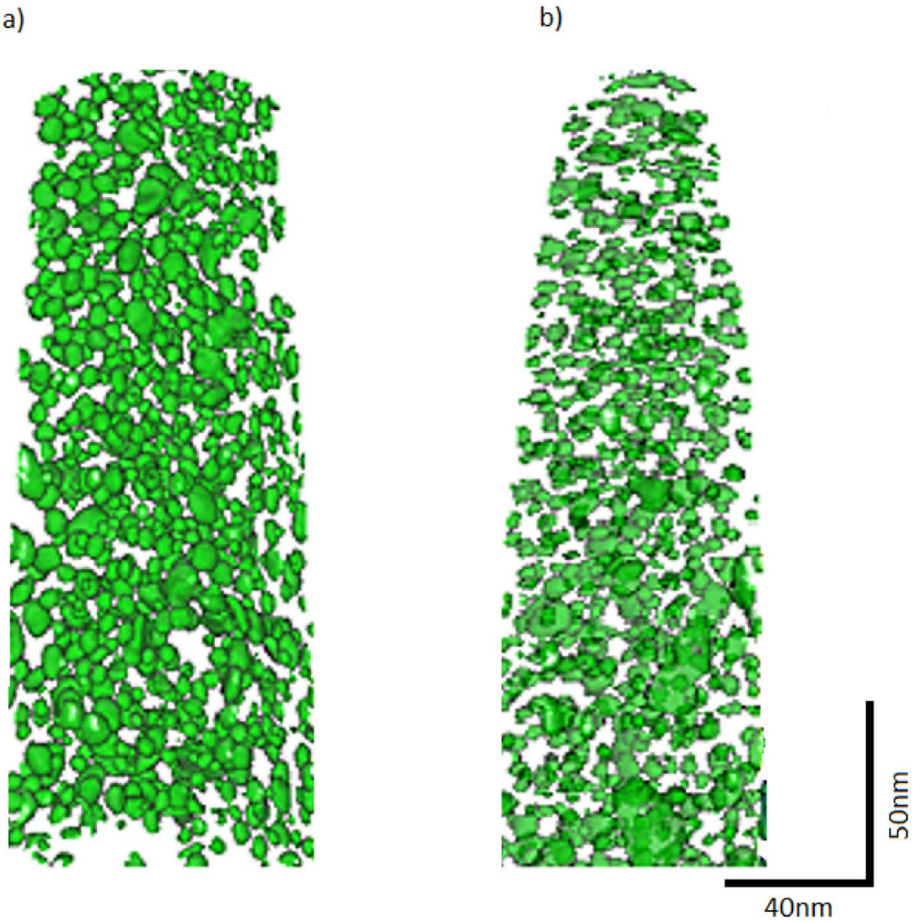

Fig. 5. APT of β-phase at an isoconcentration of 15% Ni aged 5 h at 540 °C: a) F1E-Lβ and b) F1E.

F1E, the 'matrix' includes larger anomalies such as ~1 μm 'super laves' which are outside the *q* range measured. As such the matrix was modelled using a Guinier-Porod function. This function was not used in the calculation of volume fraction of the precipitate populations. To do this APT was used to determine the composition of each precipitate and adjacent matrix as such defining the scattering length densities which are listed in Table 3 (see Section 3 for APT details). The scattering length density was not refined, consequently reducing the fitted variables to the size and volume fraction of each of the three precipitate populations (see Appendix).

From APT, SEM and TEM observations shape functions were chosen, with the two laves phases modelled by ellipses and the β-phase by a sphere. The model used to analyse the SANS spectra consisted of a Guinier Porod + Ellipse + Ellipse + Sphere model with a polydispersity of 0.2. The SANS model used in this work contains a number of variables including the size and volume fraction of the three precipitate populations in addition to the matrix (see Appendix for refined parameters). From APT and TEM conducted at 7.5 h, there precipitate populations are observed to be on the scale of ~100 nm for the laves remnant from austenitization, with the nucleating laves and β-phase observed to be ~30 nm and ~5 nm respectively. SANS model outputs were obtained through fitting the model progressively over aging times which were then compared to known precipitate size and volume fractions at 0 h and 7.5 h aging obtained from APT, SEM and TEM for each chemistries. Fitting parameters and example fits are shown in the Appendix demonstrating the accuracy and stability of the SANS modelling.

6. SANS Results

6.1. F1E-Lβ

F1E-Lβ has been formulated specifically to restrict the growth of β-phase precipitates by reducing the available Al. In Fig. 1, F1E-Lβ has minimal Laves 1 present after austenitization (~0.3%) and experiences precipitate growth during aging similar to F1E including lack of Laves 1 growth for aging at 520 °C [3]. The size and volume fraction of the Laves 1 is confirmed via TEM shown in Fig. 2.

Fig. 3 shows the evolution of laves that nucleate and grow during aging, nominally Laves 2. Compared to F1E, F1E-Lβ has an unexpected reduction in Laves 2. It is though this may occur due to the reduced Al influencing the stability of the nucleating laves which has been seen in other Fe systems [22].

Looking at the β-phase in Fig. 4, this precipitate volume fraction peaks at longer aging times with higher temperatures. Contrary to expectation, the β-phase of F1E-Lβ is greater than that seen F1E even though this chemistry has less of the critical β-phase forming element Al. Confirming this observation, Fig. 5 shows APT taken at 5 h aging at 540 °C where the β-phase precipitates are larger and more numerous than that seen in F1E [3]. It is hypothesised the reduction in Laves 2 results in more β-phase forming elements being available and therefore producing an unexpected increase in β-phase precipitates.

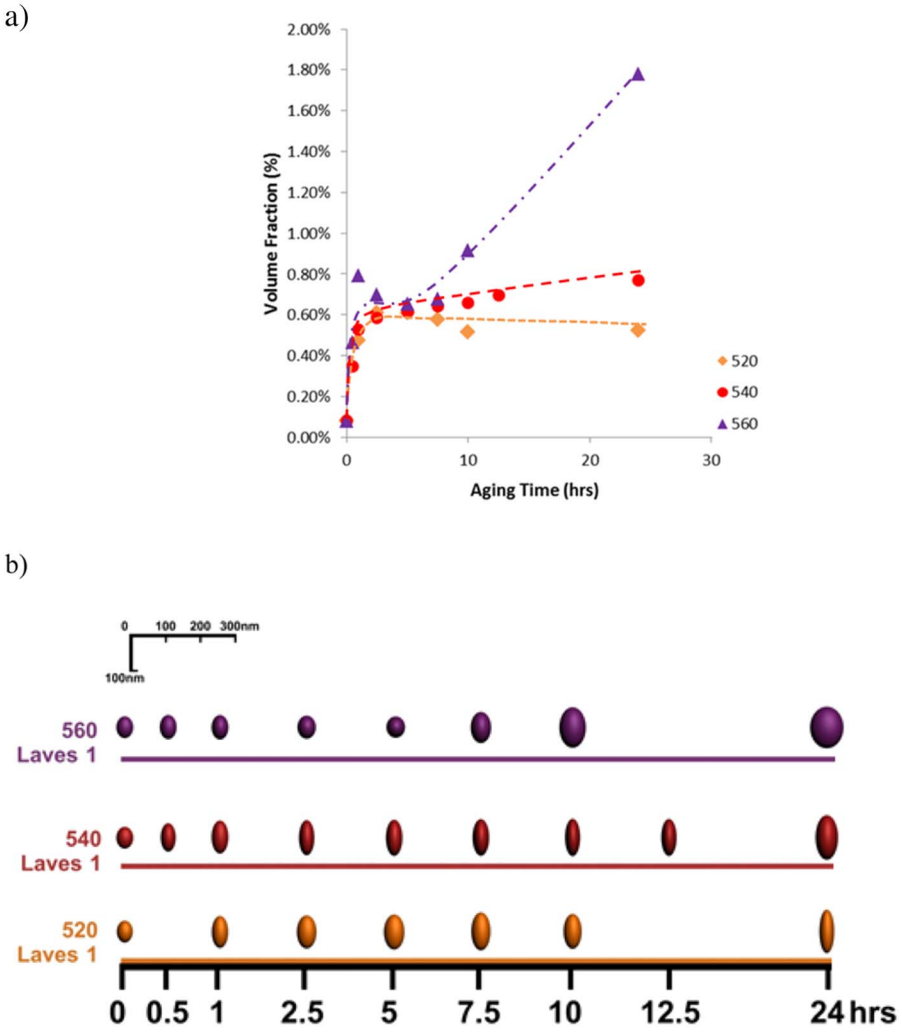

Fig. 6. F1E-LL Laves 1: aging temperature and time dependence a) volume fraction, and, b) size.

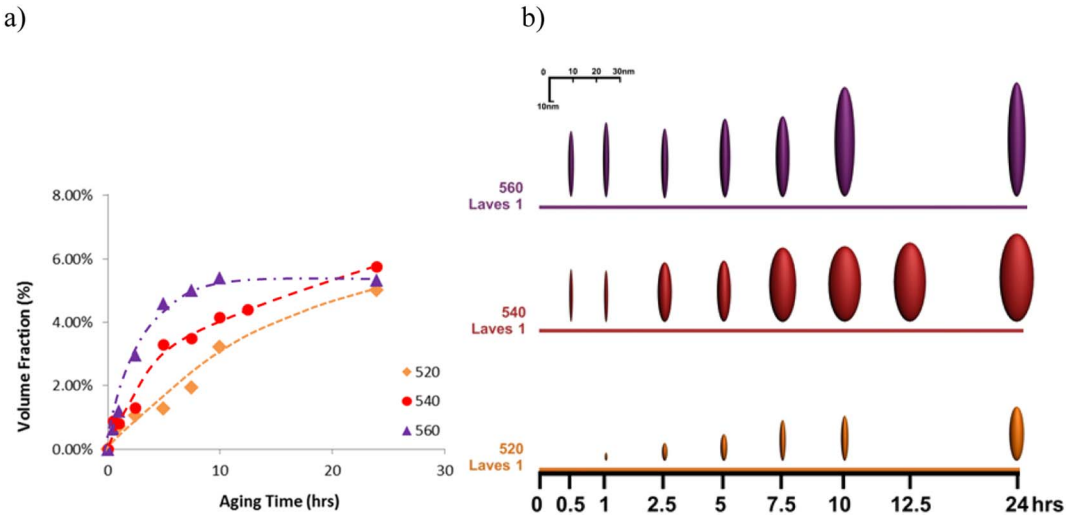

Fig. 7. F1E-LL Laves 2: aging temperature and time dependence a) volume fraction, and, b) size.

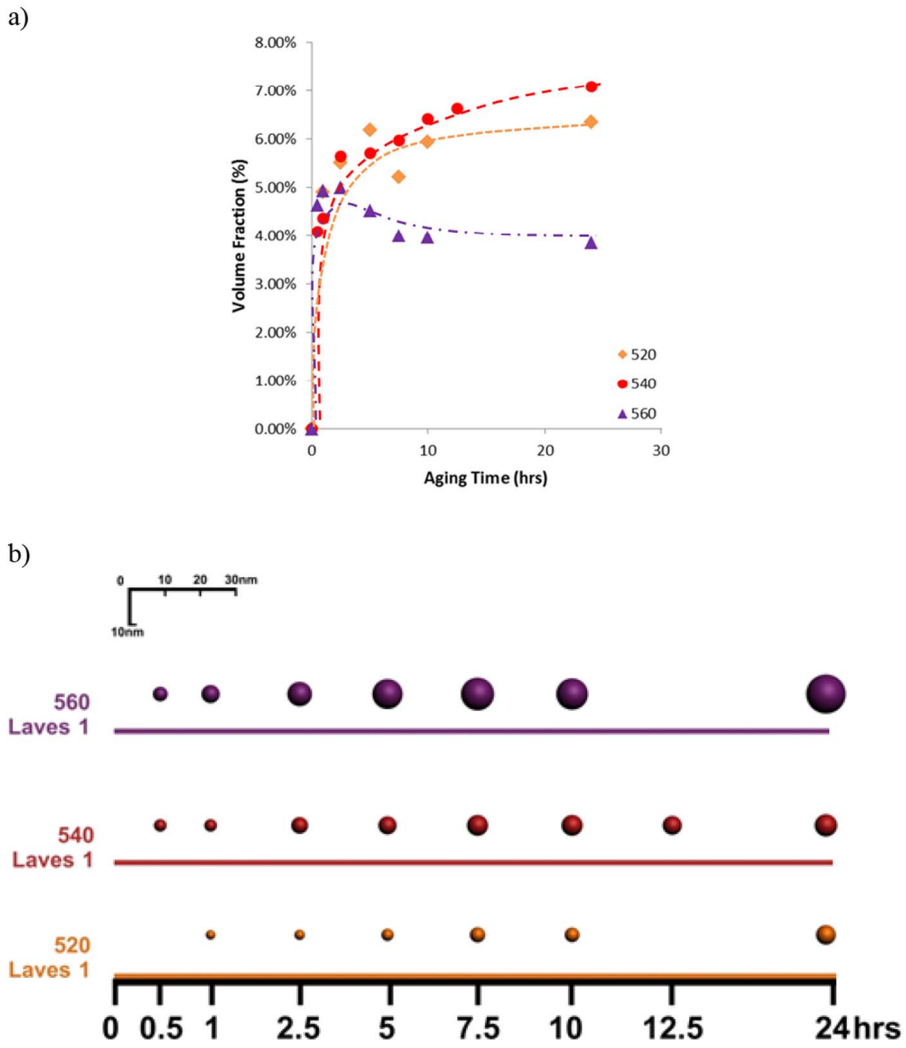

Fig. 8. F1E-LL β-phase: aging temperature and time dependence a) volume fraction, and, b)

6.2. F1E-LL

F1E-LL has reduced Mo and W which are crucial elements in forming laves precipitates. Fig. 6 shows the evolution of Laves 1 for F1E-LL where we see a significant reduction of ~50% in Laves 1 compared to F1E and F1E-Lβ. With aging, higher temperatures increase precipitation growth but still results in a minimal population of less 2% Laves 1 seen after 24 h.

In Fig. 7, Laves 2 peaks at ~5% volume fraction with higher temperatures resulting in the volume fraction peaking earlier. This population of Laves 2 is similar to that seen in F1E-Lβ, and half that seen in F1E demonstrating the reduction in Mo and W impacts the growth and development of both laves precipitate populations.

Given F1E-LL chemistry is targets laves phase precipitation, the β-phase is expected to be largely unaffected. From Fig. 8 we see that the β-phase is similar to F1E-Lβ. Higher aging temperature results in less β-phase potentially due to competition for elements with the laves phases.

6.3. F1E-NL

From Section 3 there is a marked difference in chemistry of the laves phase for F1E-NL with its significant reduction in Mo and W and increase in Cr. In Fig. 9, APT of F1E-NL aged for 5 h at 540 °C shows the small Cr rich laves phase.

In this variant chemistry only one population of laves was observed

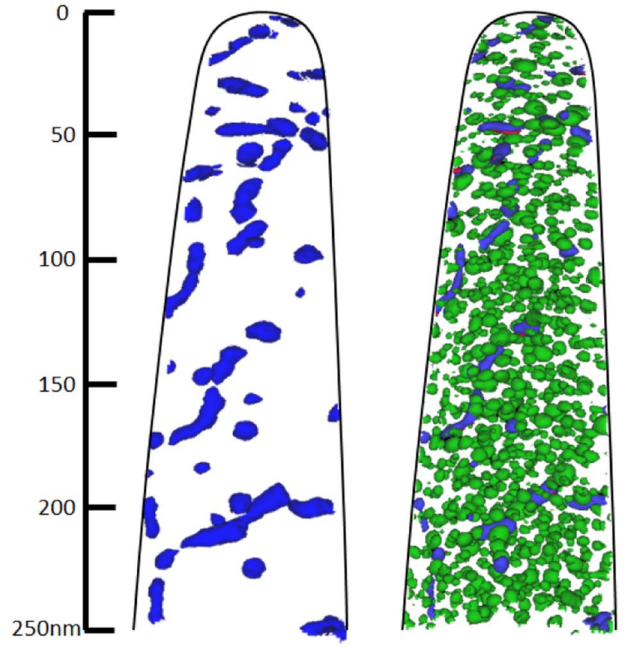

Fig. 9. APT F1E-NL aged 5 h at 540 °C: Purple is Cr rich laves, and Green is β-phase. (For interpretation of the references to color in this figure legend, the reader is referred to the web version of this article.)

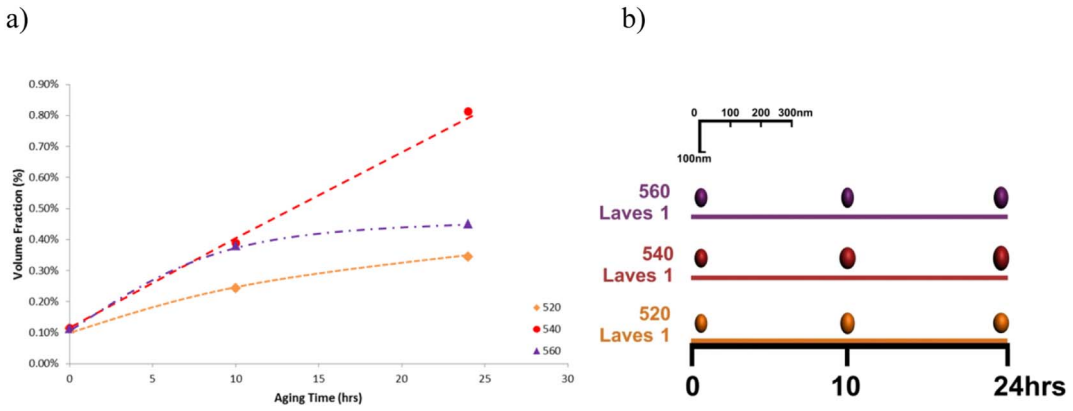

Fig. 10. F1E-NL Laves 1: aging temperature and time dependence a) volume fraction, and, b) size.

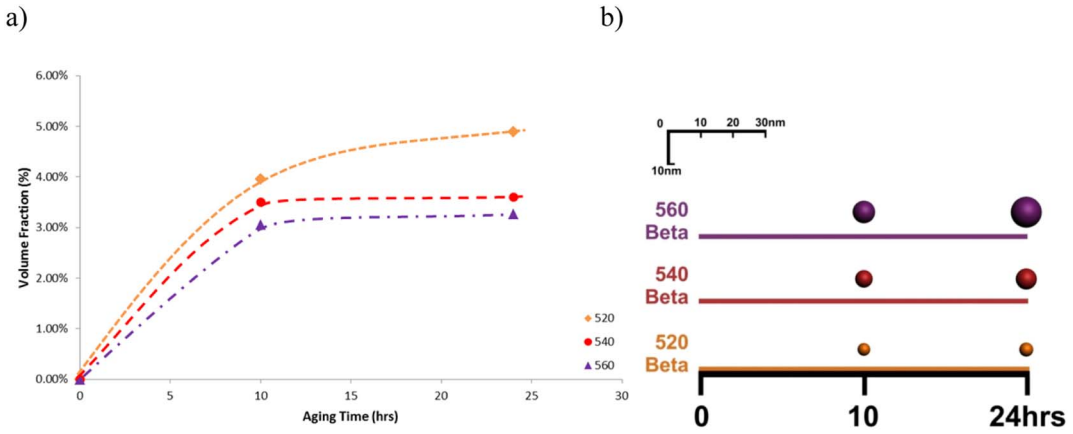

Fig. 11. F1E-NL β-phase: aging temperature and time dependence a) volume fraction, and, b) size.

and thus the SANS model reduced to a Guinier Porod + Ellipse + Sphere function. As such, Fig. 10 shows the population and size of Laves 1 precipitates. These laves are both significantly smaller and fewer than any other chemistry. When considering the β-phase in Fig. 11, it is comparable with F1E-Lβ and F1E-LL and again higher than that seen in F1E meaning the β-phase is largely unaffected by the significantly reduced Mo and W, or, the Cr rich chemistry of the resulting laves.

7. Discussion

Having characterised the precipitates through APT and SANS, we examine the mechanical properties of these variant chemistry maraging steels. Experimental details of mechanical testing is as follows:

- Hardness measurements were performed on 20 × 20 × 5 mm blanks mounted Bakelite and polished, where 10 hardness measurements were taken using a 15 kN load.
- Tensile Testing was carried out at room temperature in accordance with BS EN ISO 6892 using a Zwick electric screw machine.
- Constant stress creep tests were performed on a 15:1 Andrade-Chalmers constant stress cam creep machine.

All tests were carried out at SMaRT, Swansea University [23]. Samples were austenitized at temperatures described in the SANS Results and Appendix, then aged at 540 °C. Tensile, hardness and creep properties of F1E, F1E-Lβ, F1E-LL and F1E-NL are shown in Fig. 12.

The hardness of each variant chemistry is shown in Fig. 12a. For all chemistries, hardness values peak at 10 h of aging which coincides with the maximum/plateau of precipitate populations. F1E-Lβ shows the greatest increase in hardness. The greater increase in hardness is thought to occur due to both the β-phase and Laves 2 populations peaking at the same time unlike in all other chemistries.

From tensile results in Fig. 12b, there is only a small variation in Young's modulus between chemistries with the variant chemistries producing a slightly stiffer material compared to F1E. Considering the UTS, chemistries with the highest UTS have the greatest number of total precipitates which is determined by the Laves 2 population. Additionally, the modified chemistries demonstrate a substantial increase in ductility over F1E. This correlates to the variant chemistries having fewer overall precipitates compared to F1E (Laves 1 and 2 specifically).

From Fig. 12c, F1E has a substantially longer creep life than any of the variant chemistries reversing the ductility trend seen in tensile testing. F1E is known to have the highest in grain precipitate population, Laves 1, which would hinder dislocations under creep conditions.

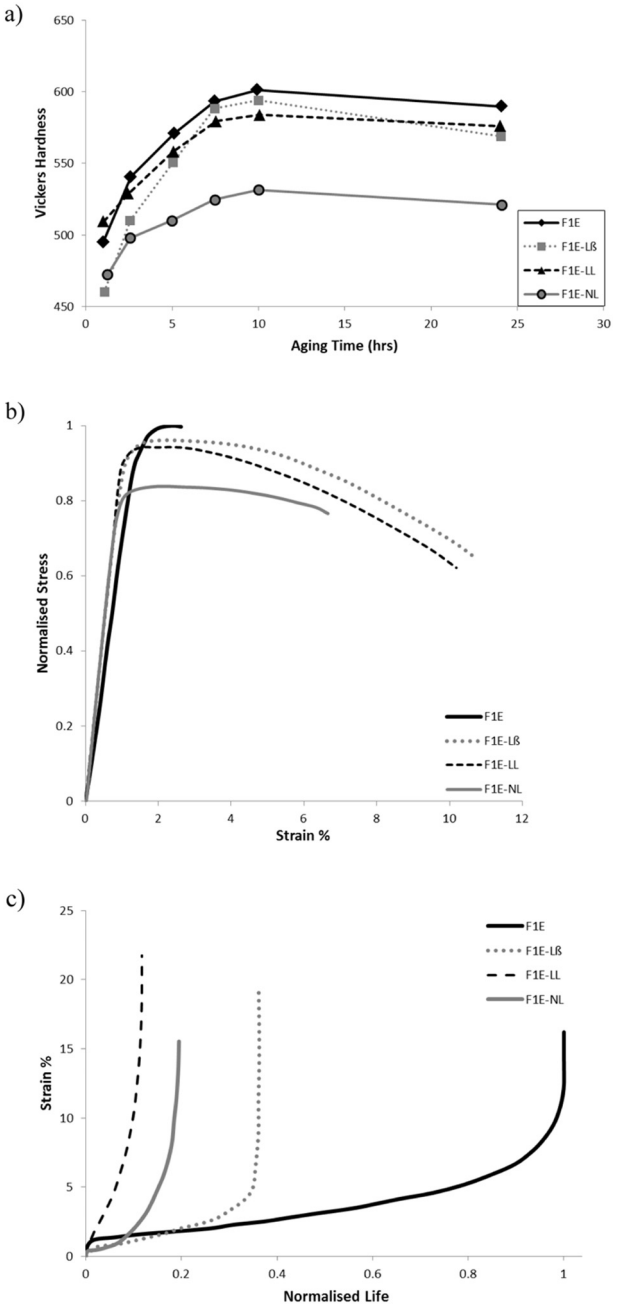

Fig. 12. Mechanical Properties a) Vickers Hardness aged at 540 °C, b) Relative Tensile Strength aged 540 °C for 7.5 h, and c) Relative Creep Life at 800 MPa 500 °C aged 540 °C for 7.5 h.

The variant chemistries have less precipitates and substantially shorter creep lives. Notably, F1E-LL exhibits a different creep curve shape and substantially higher minimum creep rate suggesting a different creep mechanism which is currently unidentified.

8. Conclusions

F1E is a maraging steel that derives its mechanical properties from precipitates making it arguably an iron based superalloy. In this work three variations of F1E were studied; F1E-Lβ, F1E-LL and F1E-NL each with reductions in specific elements linked to either laves or β-phase precipitates. From APT there was little variation in precipitate chemistry except for F1E-NL which had an unusual Cr rich laves phase. From SANS, the precipitate size and populations were determined for a range of aging times and temperatures. All variant chemistries had increased β-phase populations compared to F1E. The F1E-Lβ had a reduction in Laves 2 population, while F1E-LL had a reduction in both Laves 1 and Laves 2. F1E-NL had only a small Laves 1 population. Overall, reducing Mo and W resulted in a decrease both laves populations within the material. Reducing Al, the β-phase forming element, reduced the Laves 2. Correlating precipitate populations with mechanical properties, for all chemistries peak hardness was achieved at ~10 h aging coinciding with peaks in precipitate populations. Higher UTS correlates with a higher precipitate population, and tensile ductility is increased for lower precipitate populations. Creep sees the higher in grain precipitate chemistries (high in Laves 2 and β-phase) have longer lives potentially due to precipitate interaction with dislocations. From this study the impact of overall composition on precipitate chemistry is examined by SANS for a range of aging temperature and times. The hardness, tensile and creep properties are then able to be examined with respect to knowledge of the precipitates thus demonstrating a multi-scale approach to characterising and potentially designing novel high performance maraging steels that can be considered iron based superalloys.

Acknowledgements

This work has been funded by the Rolls-Royce plc. and the Strategic Partnership in Structural metallic systems for advanced gas turbine applications, EPSRC (EP/H500383/1). We acknowledge the support of the Australian Centre for Neutron Scattering, Australian Nuclear Science and Technology Organisation, in providing neutron research facilities and support especially the help from E. P. Gilbert who provided support and advice over a number of years. Additional acknowledgement to Dr. Lin Sun for his assistance during this project.

Appendix

The following is a table of the SANS model refined parameters:

Ellipsoid 1: Laves 1 Pre-existing laves	Ellipsoid 2: Laves 2 Nucleating laves	Sphere: β-phase
R_a	R_a	R
R_b	R_b	Scale, S
Scale, E_1	Scale, E_2	

This appendix contains the tabulated values used in Figs. 1, 3, 4, 6–8, 10 and examples of SANS fits. Each table has the austenitization and aging temperature at the top in °C, with aging time listed in hrs, lengths in nm, and volume fraction in %.

A.1. F1E-Lβ

925-520						
Aging time	0	1	2.5	5	7.5	10
Pre-existing laves						
R_a	3.4 ± 0.2	24.8 ± 2.5	27.1 ± 1.0	38.6 ± 1.9	33.1 ± 0.8	30.3 ± 0.6
R_b	7.5 ± 1.0	31.3 ± 2.2	30.8 ± 0.7	58.3 ± 3.3	66.8 ± 2.6	77.3 ± 4.5
Volume	0.3 ± 0.1	0.4 ± 0.0	0.4 ± 0.1	1.0 ± 0.0	2.3 ± 0.1	2.0 ± 0.0
Nucleating laves						
R_a	–	1.8 ± 0.0	0.8 ± 0.0	1.2 ± 0.0	1.4 ± 0.0	1.6 ± 0.0
R_b	–	4.0 ± 0.0	4.8 ± 0.0	5.6 ± 0.0	6.9 ± 0.0	8.9 ± 0.0
Volume	–	2.8 ± 0.3	6.4 ± 1.3	7.7 ± 0.7	8.7 ± 1.0	8.0 ± 1.0
Beta						
R	–	1.4 ± 0.0	1.8 ± 0.0	2.5 ± 0.0	2.9 ± 0.0	2.9 ± 0.1
Volume	–	3.7 ± 0.7	4.2 ± 0.8	4.5 ± 0.6	4.6 ± 1.8	4.0 ± 1.6

925-540					
Aging time	1	2.5	5	7.5	10
Pre-existing laves					
R_a	38.0 ± 0.5	40.9 ± 0.5	52.1 ± 2.8	56.9 ± 2.0	54.0 ± 1.7
R_b	59.0 ± 1.1	58.0 ± 0.6	50.2 ± 2.0	62.4 ± 0.7	51.6 ± 1.1
Volume	1.8 ± 0.2	2.0 ± 0.5	2.6 ± 1.0	2.8 ± 1.1	4.2 ± 1.3
Nucleating laves					
R_a	1.7 ± 0.0	1.5 ± 0.0	2.9 ± 0.0	3.4 ± 0.0	3.6 ± 0.1
R_b	4.5 ± 0.0	7.9 ± 0.0	10.7 ± 0.1	13.8 ± 0.1	14.7 ± 0.1
Volume	4.3 ± 0.2	6.1 ± 0.4	6.7 ± 0.4	7.5 ± 0.4	7.3 ± 1.6
Beta					
R	2.4 ± 0.0	3.0 ± 0.0	2.4 ± 0.0	2.7 ± 0.0	2.9 ± 0.0
Volume	1.2 ± 0.5	2.7 ± 0.5	5.0 ± 0.7	4.4 ± 0.7	4.4 ± 0.3

925-560					
Aging time	1	2.5	5	7.5	10
Pre-existing laves					
R_a	27.5 ± 1.1	48.9 ± 3.3	53.5 ± 3.2	62.7 ± 2.6	60.4 ± 6.0
R_b	32.0 ± 0.8	65.3 ± 3.9	55.9 ± 2.1	60.8 ± 1.1	60.6 ± 3.0
Volume	1.3 ± 0.3	1.5 ± 0.1	1.5 ± 0.1	1.7 ± 0.1	2.5 ± 0.1
Nucleating laves					
R_a	1.6 ± 0.0	2.7 ± 0.0	2.7 ± 0.0	3.5 ± 0.0	5.6 ± 0.0
R_b	6.9 ± 0.0	9.0 ± 0.0	10.3 ± 0.1	13.1 ± 0.1	22.3 ± 0.2
Volume	4.0 ± 0.4	5.3 ± 0.4	6.3 ± 0.3	7.1 ± 0.4	8.6 ± 0.6
Beta					
R	0.8 ± 0.0	2.9 ± 0.0	3.4 ± 0.0	2.8 ± 0.0	4.3 ± 0.0
Volume	1.0 ± 0.3	1.6 ± 0.0	4.4 ± 0.1	5.3 ± 0.1	5.3 ± 0.1

A.2. F1E-LL

900-520							
Aging time	0	1	2.5	5	7.5	10	24
Pre-existing laves							
R_a	24.3 ± 0.8	25.8 ± 0.4	29.3 ± 0.4	29.5 ± 0.6	28.1 ± 0.7	27.4 ± 0.8	25.1 ± 0.7
R_b	31.5 ± 0.9	46.9 ± 2.0	28.3 ± 1.1	51.2 ± 1.4	59.5 ± 2.7	51.6 ± 2.3	63.9 ± 6.4
Volume	0.1 ± 0.0	0.5 ± 0.0	0.6 ± 0.0	0.6 ± 0.0	0.6 ± 0.1	0.6 ± 0.1	
Nucleating laves							
R_a	–	0.6 ± 0.0	1.2 ± 0.0	1.5 ± 0.0	1.3 ± 0.0	1.8 ± 0.0	3.4 ± 0.0
R_b	–	1.8 ± 0.1	3.8 ± 0.0	5.6 ± 0.1	8.8 ± 0.1	8.6 ± 0.1	11.6 ± 0.0
Volume	–	0.7 ± 0.0	1.1 ± 1.0	1.3 ± 0.0	2.0 ± 0.0	3.2 ± 0.0	5.0 ± 0.1
Beta							
R	–	1.4 ± 0.0	1.5 ± 0.0	1.8 ± 0.0	2.1 ± 0.0	2.0 ± 0.0	2.4 ± 0.0
Volume	–	4.9 ± 0.4	5.5 ± 0.3	6.2 ± 0.3	5.2 ± 0.2	6.0 ± 0.2	6.4 ± 0.1

900-540								
Aging time	0.5	1	2.5	5	7.5	10	12.5	24
Pre-existing laves								
R_a	22.3 ± 0.7	25.0 ± 0.6	22.7 ± 0.4	24.5 ± 0.3	24.2 ± 0.8	22.7 ± 0.7	22.1 ± 0.7	33.0 ± 1.8
R_b	41.2 ± 2.3	48.3 ± 2.9	49.1 ± 2.1	52.1 ± 1.2	52.6 ± 2.8	56.6 ± 3.4	52.6 ± 3.1	64.7 ± 6.3
Volume	0.4 ± 0.0	0.5 ± 0.0	0.6 ± 0.0	0.6 ± 0.0	0.6 ± 0.1	0.7 ± 0.1	0.7 ± 0.0	0.8 ± 0.1
Nucleating laves								
R_a	0.9 ± 0.0	0.9 ± 0.0	3.4 ± 0.0	3.2 ± 0.4	6.0 ± 0.0	7.1 ± 0.0	7.2 ± 0.0	7.5 ± 0.0
R_b	15.0 ± 0.6	11.1 ± 0.4	12.8 ± 0.1	13.2 ± 0.1	15.9 ± 0.1	16.0 ± 0.1	16.9 ± 0.1	18.8 ± 0.1
Volume	0.9 ± 0.3	0.8 ± 0.0	1.3 ± 0.1	3.3 ± 0.2	3.5 ± 0.1	4.1 ± 0.1	4.4 ± 0.2	5.8 ± 0.3
Beta								
R	1.8 ± 0.0	1.8 ± 0.0	2.4 ± 0.0	2.6 ± 0.0	3.0 ± 0.0	3.1 ± 0.0	2.7 ± 0.0	3.2 ± 0.0
Volume	4.1 ± 0.1	4.4 ± 0.1	5.6 ± 0.1	5.7 ± 0.1	6.0 ± 1.1	6.4 ± 1.1	6.6 ± 0.1	7.1 ± 0.1

900-560							
Aging time	0.5	1	2.5	5	7.5	10	24
Pre-existing laves							
R_a	24.0 ± 0.4	24.2 ± 0.3	31.8 ± 1.2	29.1 ± 3.0	44.7 ± 1.0	58.0 ± 2.5	60.7 ± 6.9
R_b	35.1 ± 1.1	35.6 ± 0.7	32.6 ± 0.4	29.0 ± 1.5	30.5 ± 0.2	28.9 ± 0.2	58.8 ± 2.0
Volume	0.8 ± 0.1	0.7 ± 0.1	0.8 ± 0.1	0.7 ± 0.1	0.7 ± 0.1	0.9 ± 0.1	1.8 ± 0.3
Nucleating laves							
R_a	1.2 ± 0.0	1.4 ± 0.0	1.6 ± 0.0	2.3 ± 0.0	2.8 ± 0.0	4.4 ± 0.0	4.0 ± 0.0
R_b	14.2 ± 0.9	16.1 ± 0.5	14.8 ± 0.2	16.8 ± 0.2	17.4 ± 0.2	23.1 ± 0.3	25.0 ± 0.5
Volume	0.6 ± 0.1	1.2 ± 0.3	3.0 ± 0.2	4.6 ± 0.2	5.0 ± 0.3	5.4 ± 0.3	5.3 ± 0.4
Beta							
R	2.1 ± 0.0	2.6 ± 0.0	3.5 ± 0.0	4.3 ± 0.0	4.7 ± 0.0	4.5 ± 0.0	5.5 ± 0.1
Volume	4.6 ± 0.2	4.9 ± 0.1	5.3 ± 0.1	4.5 ± 0.0	4.0 ± 0.2	4.0 ± 0.1	3.9 ± 0.2

SANS fits are shown for F1E-LL aging at 540 °C as an example of model fit to data; data in blue and model in red, as well as, the normalised error i.e. residuals. Figures are listed in a 3 number format A-B-C where A = austenitization temperature (°C), B = aging temperature (°C), and C = aging time (hrs).

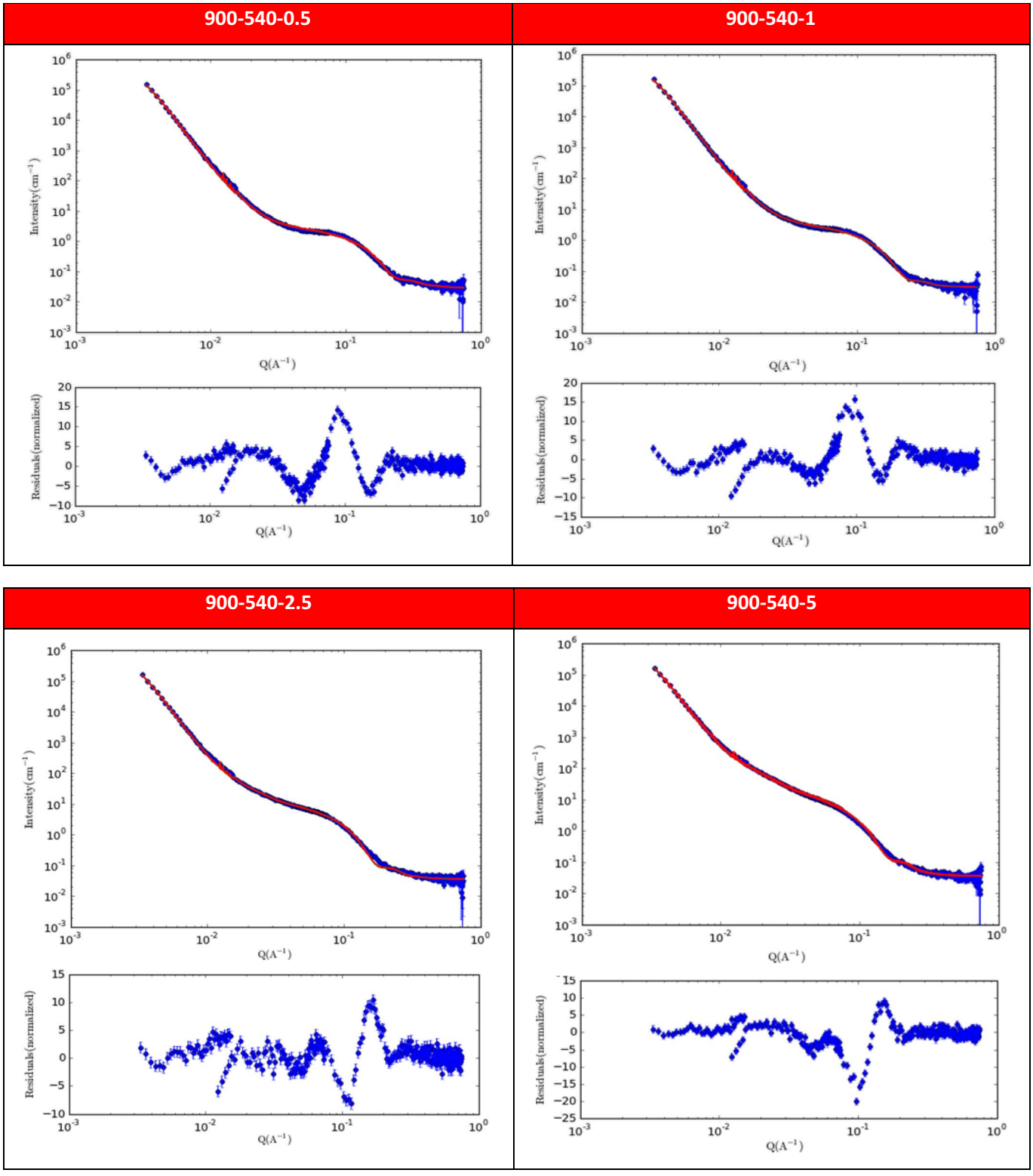
900-540-0.5
900-540-1
900-540-2.5
900-540-5
Intensity(cm^{-1})
Residuals(normalized)
Q(A^{-1})

900-540-7.5	900-540-10
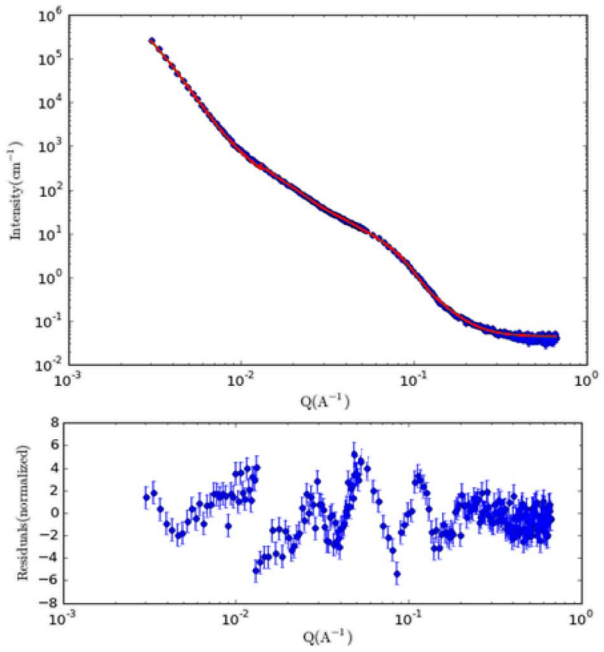	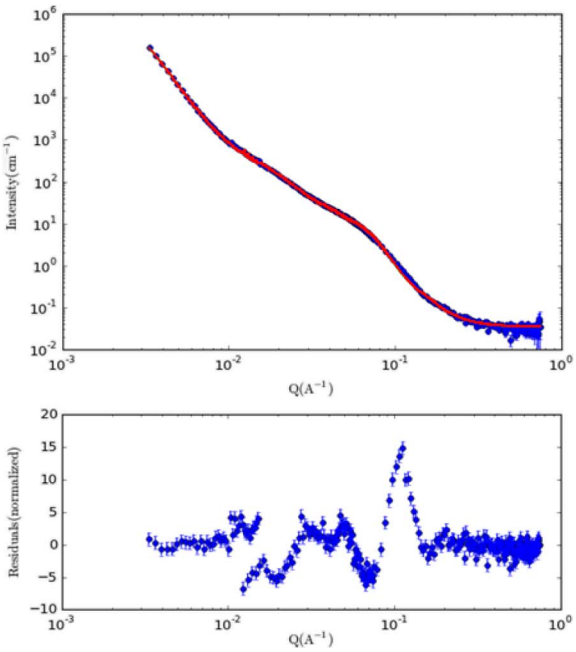
900-540-12.5	**900-560-24**
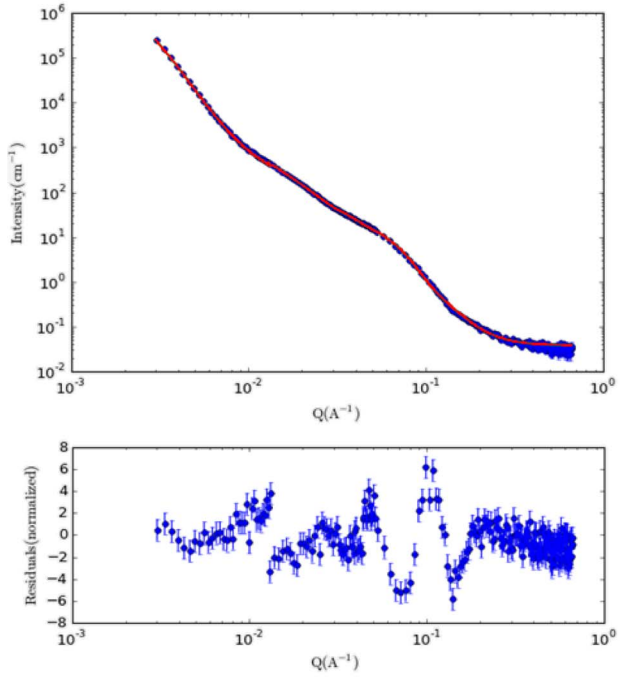	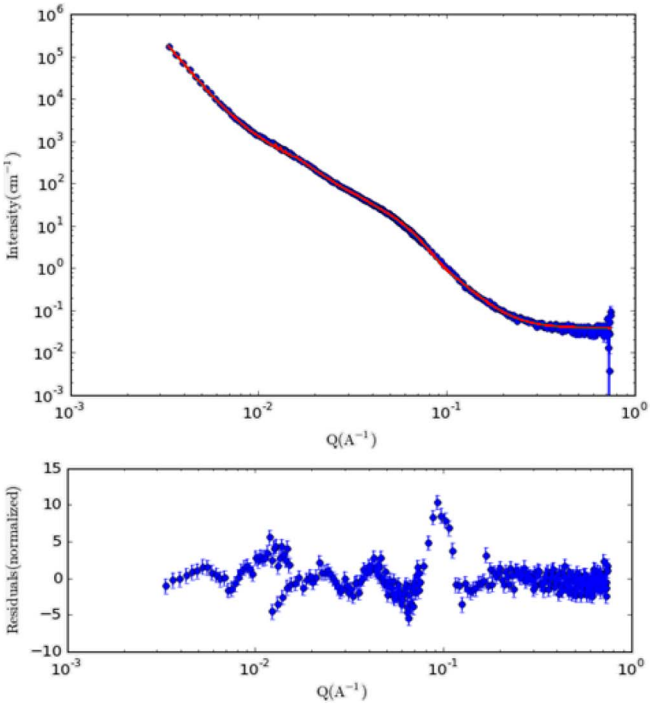

A.3. F1E-NL

840-520			
Aging time	0	10	24
Laves			
R_a	21.6 ± 0.4	24.3 ± 0.6	26.1 ± 0.7
R_b	31.4 ± 0.5	35.1 ± 1.1	33.1 ± 0.7
Volume	0.1 ± 0.0	0.2 ± 0.1	0.3 ± 0.1
Beta			
R	2.0 ± 0.0	2.2 ± 0.0	2.7 ± 0.0
Volume	4.1 ± 0.1	4.4 ± 0.1	5.6 ± 0.1

840-540		
Aging time	10	24
Laves		
R_a	27.5 ± 0.8	26.4 ± 0.0
R_b	36.5 ± 1.0	40.8 ± 1.0
Volume	0.4 ± 0.1	0.8 ± 0.2
Beta		
R	2.7 ± 0.0	3.3 ± 0.0
Volume	3.5 ± 0.1	3.6 ± 0.1

840-560		
Aging time	10	24
Laves		
R_a	21.4 ± 0.6	24.6 ± 1.5
R_b	34.8 ± 1.3	36.0 ± 0.5
Volume	0.4 ± 0.2	0.5 ± 0.2
Beta		
R	3.5 ± 0.0	4.8 ± 0.0
Volume	3.0 ± 0.1	3.3 ± 0.1

References

[1] D.E.R. Petty, Martensite: Fundamentals and Technology, Longman, London, 1970.
[2] M.P. Boyce, Gas Turbine Engineering Handbook, 3rd Edition, Gulf Professional Publishing, Oxford, 2006.
[3] V. Gray, D. Galvin, L. Sun, E.P. Gilbert, T. Martin, P. Hill, M. Rawson, K.P. Perkins, Precipitation in a novel maraging steel F1E: a study of austenitization and aging using small angle neutron scattering, Mater. Charact. 129 (2017) 270–281.
[4] S. McAdams, PhD Thesis: The Mechanical Characterisation of a High Strength, Creep Resistant Steep for Aerospace Applications, Swansea University, April 2014.
[5] H.J. Rack, D. Kalish, Improvement in fatigue resistance of 18Ni(350) maraging steel through thermo-mechanical treatments, Metall. Trans. A. 5 (1974) 685–694.
[6] W. Sha, Y. He, K. Yang, D.J. Cleland, Microstructure and mechanical properties of a 2000 MPa Co-free maraging steel after ageing at 753 K, Metall. Trans. A. 35 (2004) 2747–2755.
[7] Rolls-Royce plc., PO Box 31, Derby DE24 8BJ, UK.
[8] ATI Specialty Metals: Allvac, Monroe NC 281110, USA, https://www.atimetals.com/businesses/ATISpecialtyMaterials/Pages/default.aspx.
[9] B. Gault, Atom Probe Microscopy, Springer, New York, 2012.
[10] R.H. Davies, A.T. Dinsdale, J.A. Gisby, J.A.J. Robinson, S.M. Martin, MDATA-thermodynamics and phase equilibrium software from the National Physical Laboratory, Calphad 26 (2002) 229–271.
[11] E.P. Gilbert, J.C. Schulz, T.J. Noakes, Quokka'–the small-angle neutron scattering instrument at OPAL, Physica B 385–386 (2006) 1180–1182.
[12] S.R. Kline, Reduction and analysis of SANS and USANS data using IGOR Pro, J. Appl. Crystallogr. 39 (2006) 895–900.
[13] Irena for Igor, Argonne National Laboratory, Used 28/11/2014, http://usaxs.xray.aps.anl.gov/staff/ilavsky/irena.html.
[14] Quokka User Manual, Version: October 2015 http://www.ansto.gov.au/cs/groups/corporate/documents/document/mdaw/mdm4/~edisp/acs079538.pdf.
[15] SaSview Version 3.0.0, Installed 15/01/2015 http://www.sasview.org.
[16] A. Guinier, G. Fournet, Small-angle Scattering of X-rays, John Wiley and Sons, New York, 1955.
[17] O. Glatter, O. Kratky, Small-angle X-ray Scattering, Academic Press, London, 1982.
[18] A. Guinier, G. Fournet, Small-angle Scattering of X-rays, John Wiley and Sons, New York, 1955.
[19] SANS Model Function Documentation Version 4, Accessed 20/01/2015, February 2008. http://www.ncnr.nist.gov/programs/sans/data/Download/SANS_Model_Docs_v4.00.pdf, .
[20] L.A. Feigin, D.I. Svergun, Structure Analysis by Small-angle X-ray and Neutron Scattering, Plenum Press, New York, 1987.
[21] S. Kline, A. Munter, Ellipsod Model, Accessed 04/09/2015 http://www.ncnr.nist.gov/resources/sansmodels/Ellipsoid.html.
[22] F. Stein, M. Palm, G. Sauthoff, Structure and stability of Laves phases. Part I. Critical assessment of factors controlling Laves phase stability, Intermetallics 12 (2004) 713–720.
[23] Swansea Materials Research & Testing, http://www.smart-swansea.com.